Journal of ELECTRONIC MATERIALS, Vol. 45, No. 11, 2016
DOI: 10.1007/s11664-016-4780-2

Electrical Conductivity, Thermal Behavior, and Seebeck Coefficient of Conductive Films for Printed Thermoelectric Energy Harvesting Systems

KRISHNAMRAJU ANKIREDDY,[1,4] AKANKSHA K. MENON,[2] BRIAN IEZZI,[1] SHANNON K. YEE,[2] MARK D. LOSEGO,[3] and JESSE S. JUR[1,5]

1.—Department of Textile Engineering, Chemistry and Science, North Carolina State University, Raleigh, NC, USA. 2.—George W. Woodruff School of Mechanical Engineering, Georgia Institute of Technology, Atlanta, GA, USA. 3.—School of Materials Science and Engineering, Georgia Institute of Technology, Atlanta, GA, USA. 4.—e-mail: krishnamraju.ankireddy@louisville.edu. 5.—e-mail: jsjur@ncsu.edu.

Printed electronics is being explored as a rapid, facile means for manufacturing thermoelectric generators (TEGs) that can recover useful electrical energy from waste heat. This work examines the relevant electrical conductivity, thermal resistance, thermovoltage, and Seebeck coefficient of printed films for use in such printed flexible TEGs. The thermoelectric performance of TEGs printed using commercially relevant nickel, silver, and carbon inks is evaluated. The microstructure of the printed films is investigated to better understand why the electrical conductivity and Seebeck coefficient are degraded. Thermal conduction is shown to be relatively insensitive to the type of metalized coating and nearly equivalent to that of an uncoated polymer substrate. Of the commercially available conductive ink materials examined, carbon–nickel TEGs are shown to exhibit the highest thermovoltage, with a value of 10.3 μV/K. However, silver–nickel TEGs produced the highest power generation of 14.6 μW [from 31 junctions with temperature difference (ΔT) of 113°C] due to their low electrical resistance. The voltage generated from the silver–nickel TEG was stable under continuous operation at 275°C for 3 h. We have also demonstrated that, after a year of storage in ambient conditions, these devices retain their performance. Notably, the electrical conductivity and Seebeck coefficient measured for individual materials were consistent with those measured from actual printed TEG device structures, validating the need for further fundamental materials characterization to accelerate flexible TEG device optimization.

Key words: Printed thermoelectric generators, energy harvesting, electrical conductivity, thermal conductivity, Seebeck coefficient, conductive films

INTRODUCTION

Technologies for recovering waste energy are paramount to reinventing the global energy economy. Heat is the most prevalent form of waste energy, and over half of such waste heat is released in low-temperature (< 250°C) streams.[1] Thermoelectric generators (TEGs) are solid-state devices that convert waste heat into more useful electrical energy via the Seebeck effect.[2] The salient features of TEG power generation include high reliability (no moving parts), silent operation, and continuous energy recovery. Drawbacks of traditional

(Received February 9, 2016; accepted June 28, 2016; published online July 26, 2016)

semiconductor- or ceramic-based TEGs include mechanical rigidity, high fabrication costs, and nonuniversal installation. Recently, researchers have capitalized on advances in printed electronics to enable low-cost printing of thermoelectric devices on flexible substrates.[3–11] These low-cost, flexible devices address many of the deficiencies found in traditional TEG designs, but final devices have markedly lower performance. Still, some estimates suggest that lower cost per watt can be achieved due to low processing and materials costs.[12,13]

Several examples of flexible and printed TEGs have been reported in literature; For example, wearable TEGs fabricated from *p*-type and *n*-type Bi_2Te_3 ink on polydimethylsiloxane substrates for the purpose of harvesting body heat generated 2.1 μW of power per eight thermoelectric (TE) couples at temperature differential (ΔT) of ~19 K.[3] A prototype, consisting of 11 TE couples, fabricated on a glass fabric using *n*-type Bi_2Te_3 and *p*-type Sb_2Te_3 generated power of 3 μW when applied on the human body with air temperature of 15°C.[4] A poly(3,4-ethylenedioxythiophene):polystyrene sulfonate (PEDOT:PSS)-coated commercial polyester fabric for the purpose of body heat energy recovery generated power of 12.3 nW per five TE strips at temperature difference of 75 K.[5] Madan et al. printed a 10-couple TEG onto a flex printed circuit board substrate using Bi-epoxy and $Bi_{0.5}Sb_{1.5}Te_3$ inks. This device produced 130 μW of power at ΔT of 70 K.[6,7]

A second consideration for such printed TEGs is to replace toxic and modestly expensive constituents such as tellurium, bismuth, thallium, and antimony;[14] For example, tellurium and thallium compounds can decompose and emit toxic vapors under high-temperature operation. While not precious metals, they are also not as earth-abundant and inexpensive as other elements such as iron, copper, aluminum, nickel, zinc or carbon. Based on these further restrictions, interest has grown in alternative printed materials, including polymeric, carbonaceous, metal oxide, and base-metal inks for low-cost and nontoxic TEGs.[15–23] One example by Jiao et al. is an inkjet-printed six-junction thermoelectric generator fabricated from polymer composites that generated thermoelectric power of 45 nW at temperature difference of 25°C.[22]

While many groups have reported printed TEG devices, mainly using traditional TEG materials such as bismuth- and tellurium-based compounds, few of these studies have focused on the fundamental transport properties of the inks—electrical conductivity, thermal conductivity, and Seebeck coefficient—that dictate device performance. Better understanding of how ink composition and print processing affect these properties will enable faster technology development. Herein we present new results probing these critical transport properties for a few different commercially available ink materials including carbon, nickel, and silver and the effect of ink composition on the properties of the TEG devices, even if the same base material (nickel) is used for two different ink formulations. Our hope is that the simple techniques described herein will inspire further exploration of these important transport properties in other conductive ink systems of interest for TEGs.

EXPERIMENTAL PROCEDURES

TEG structures were screen-printed using different combinations of inks/pastes. Note that, in this report, we use the terms "ink" and "paste" interchangeably based on the commercial descriptions. The printing technique used is the same as for flexible TEGs previously reported in literature; For example, Madan et al. reported a similar concept of printing TEGs on flexible substrates.[6] TEG devices were dispenser-printed onto flexible polyimide substrate using traditional thermoelectric materials for scalable manufacturing. The connecting leads to the TEGs were attached using silver epoxy. In our work, we screen-printed conductive materials instead of traditional thermoelectric materials and attached the connecting leads with silver epoxy. DuPont 5064H silver paste and Creative Materials carbon ink (124-43) were evaluated along with two in-house-formulated nickel pastes. These pastes were prepared by simple mixing of commercially available nickel powders, binders, and solvents. The DuPont silver paste had solids fraction of 65%.[24] The solids content of the carbon ink was not provided, but it was found to have lower viscosity than the silver paste. Self-formulated nickel paste 1 (Ni-1) was synthesized from Culox 5010 nickel powder (average powder diameter 1 μm) dispersed in α-terpineol and stabilized with polyvinylpyrrolidone (PVP, molecular weight 40,000 g/mol), which also acted as binding agent. Ni-1 had total solids content of 80% with PVP fraction of 2% at room temperature. Nickel paste 2 (Ni-2) was formulated from 1-μm- to 5-μm-sized nickel flakes purchased from Atlantic Equipment Engineer, Upper Saddle River, NJ. These nickel flakes were suspended in ethylene glycol, with PVP again used as binding agent. The total solids content of paste Ni-2 was 81% with PVP fraction of 2%. Kapton® films of 125 μm thickness were used as flexible substrates for device printing.

To evaluate fundamental materials properties, films of Ag, C, Ni-1, and Ni-2 pastes were screen-printed across the entire surface of square Kapton® or square glass substrates. These substrates were cleaned with acetone before ink printing. Films printed on 50 mm × 50 mm and 25 mm × 25 mm Kapton® substrates were used to measure the thermal transport and electrical resistance of the pastes, respectively. Films printed on 25 mm × 25 mm glass substrates were used for Seebeck coefficient measurements. Silver films were printed in one pass, while nickel and carbon films

were printed in two passes. All films required sintering to make them electrically conductive. Silver and carbon pastes were sintered at 120°C for 30 min in air, while nickel pastes were sintered at 350°C for 3 h under inert Ar environment.

Images of representative films are shown in Fig. 1a. Film microstructure and thickness were evaluated using a Phenom G1 desktop scanning electron microscope (SEM). Sheet resistance was measured with a Jandel four-point probe system equipped with an RM3-AR head. The in-plane Seebeck coefficient of these printed films was evaluated using custom-built instrumentation that measures the voltage drop of a sample suspended between two Peltier heaters having independently controlled temperature settings.[25] A Keithley 2700 DMM/7708 Mux interfaced with LabVIEW allowed data logging of the voltage drop as a function of ΔT and extraction of the Seebeck coefficient. Heat conduction was evaluated using infrared (IR) imaging to mimic operational conditions. Printed films were heated by their edge using a fixed temperature source, and IR images were captured with a FLIR-E49001 IR camera from FLIR. To calibrate for the emissivity of each conductive film, temperature was independently measured with a surface-attached thermocouple at one adjacent position. IR images were analyzed, using FLIR Tools analysis software from FLIR, to calculate temperatures at fixed incremental distances from the hot surface. An example of this experimental setup is shown in Fig. 1b.

Simple TEGs composed of 31 junctions were also fabricated on Kapton® substrates to assess electrical resistance, heat flow, Seebeck coefficient, and power generation under simulated device conditions. TEG structures were simple zigzag patterns with each leg being 20 mm long × 5 mm wide. When TEGs were printed from two inks requiring different annealing schedules, various optimized heat treatments were applied. For Ag/C or Ag/Ni TEGs, silver pastes were printed first and sintered as usual. To form Ag/C junctions, carbon legs were added, and the TEG was reannealed at 120°C for 30 min in air. If Ag/Ni junctions were desired, then nickel legs were added, and the TEG was subsequently annealed in Ar at 350°C for 3 h. In the case of C/Ni structures, nickel patterns were printed first and sintered in Ar at 350°C for 3 h, followed by carbon printing and subsequent sintering at 120°C for 30 min in air.

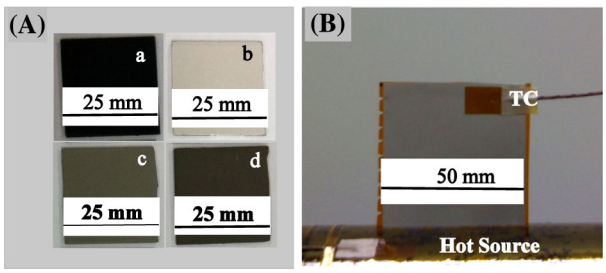

Fig. 1. Screen-printed and sintered films. (A) Printed films on glass substrates: (a) carbon, (b) silver, (c) Ni-1, and (d) Ni-2. (B) Experimental setup for measuring the temperature profile of a silver film on Kapton® substrate.

Representative images of these simple TEG devices are shown in Fig. 2. Planar TEG structures with junction combinations of Ag/Ni-1, Ag/Ni-2, C/Ag, C/Ni-1, and C/Ni-2 were evaluated. Electrical leads were attached to the TEG devices using silver epoxy after sintering. The electrical resistance of TEG structures was measured using a multimeter. Changes in the electrical resistance with increasing heat source temperature were also monitored. To measure the thermoelectric voltage, TEGs were placed on the surface of a hot source. A surface thermocouple was attached on the hot surface to monitor temperature. This temperature was used as the "hot-junction temperature." The "cold-junction temperature" was monitored with a thermocouple directly attached to the TEG. The open-circuit voltage was measured by increasing the hot source temperature from room temperature to 275°C. The Seebeck coefficient for each type of junction was calculated from the slope of the plot of open-circuit voltage versus ΔT.

The voltage difference between different TEG structures was due to the different Seebeck coefficients of the inks. The open-circuit voltage can be directly related to the junction Seebeck coefficient of the two materials used for fabricating the TEG structure:

$$V_{\text{Open}} = S_{\text{thermopile}} \times \Delta T = (S_{\text{A}} - S_{\text{B}}) \times (T_{\text{Hot}} - T_{\text{Cold}}), \quad (1)$$

where T_{Hot} is the TEG's hot-junction temperature, T_{Cold} is the TEG's cold-junction temperature, and S_{A} and S_{B} are the Seebeck coefficients of the TEG legs. The thermoelectric power generated from each TEG structure was calculated by measuring the voltage across the corresponding matching load resistance.

RESULTS AND DISCUSSION

Microstructure and Electronic Properties

Table I summarizes the electrical conductivity and Seebeck coefficient for each material uniformly screen-printed on square substrates (Fig. 1). As expected, the electrical conductivity for all printed inks was lower than the corresponding bulk values. While the carbon ink retained about half of its pure bulk conductivity, all metallic inks exhibited ≤4% of their pure bulk values. These decreases in electrical conductivity are a consequence of additives (binders), void space, and particle–particle interfaces.[26] SEM images of the surface morphology for sintered conductive films (Fig. 3) clearly exhibit these microstructural defects, including significant fractions of void space. Cross-sectional images (Fig. 4) reveal additional porosity throughout the film thickness.

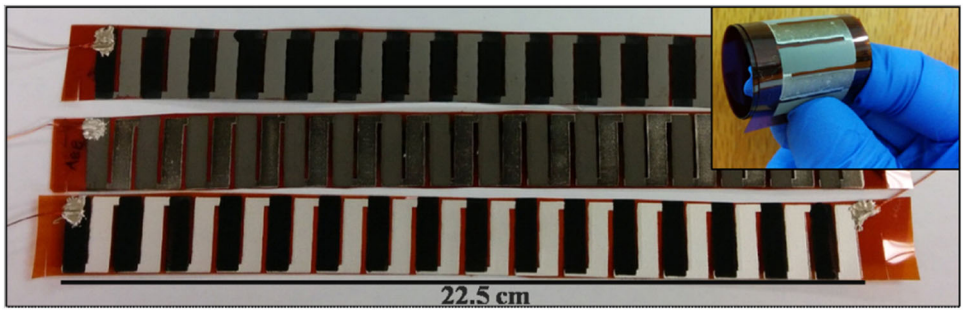

Fig. 2. Photographs of printed TEG structures on Kapton®substrate.

Table I. Electrical conductivity and Seebeck coefficient of inks as obtained from printed thin films at room temperature

Printed film	Thickness (μm)	Electrical conductivity, σ (S/m)	% of Bulk material σ[27]	Seebeck coefficient, S (μV/K)	Bulk material S (μV/K)[28]
Carbon	47	1.1×10^3	68.5%	1.8	3
Ni-1	40	1.9×10^4	0.1%	−4.5	−15
Ni-2	53	9.4×10^4	0.7%	−5.3	−15
Silver	18	2.2×10^6	4.0%	0.6	6.5

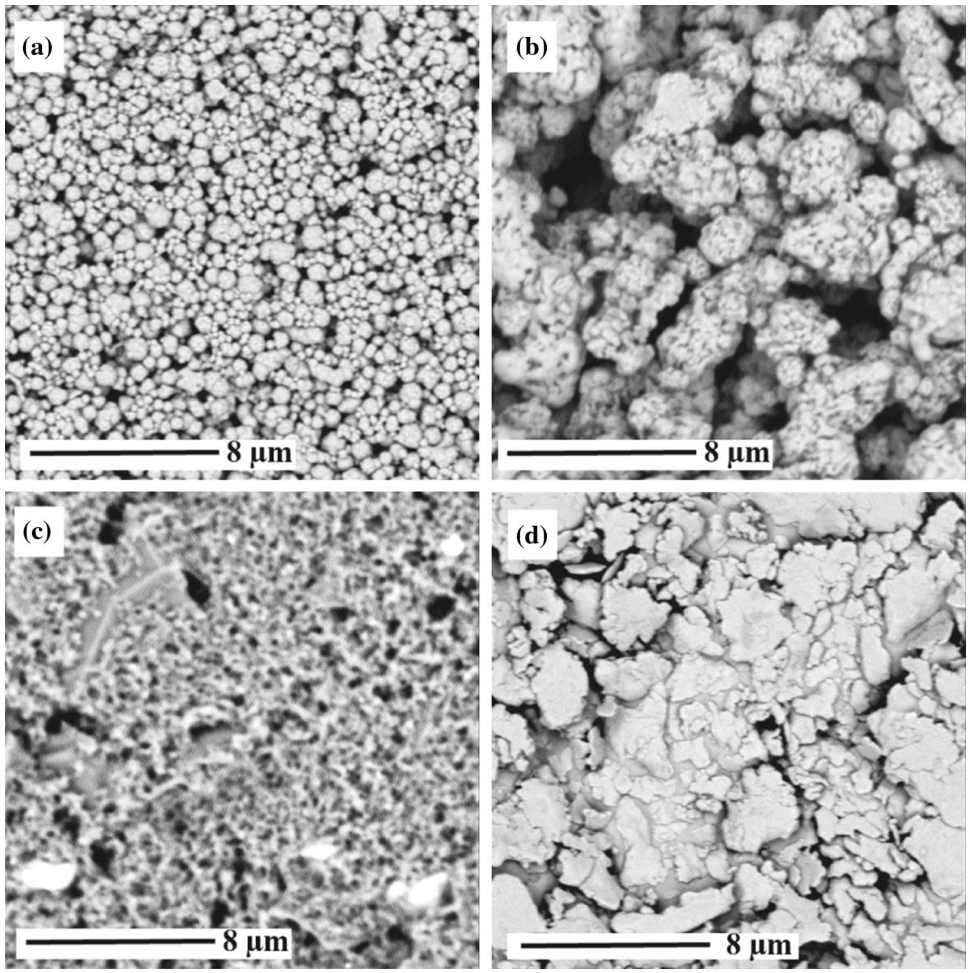

Fig. 3. SEM surface morphology images of printed films: (a) Ni-1, (b) Ni-2, (c) C, and (d) Ag.

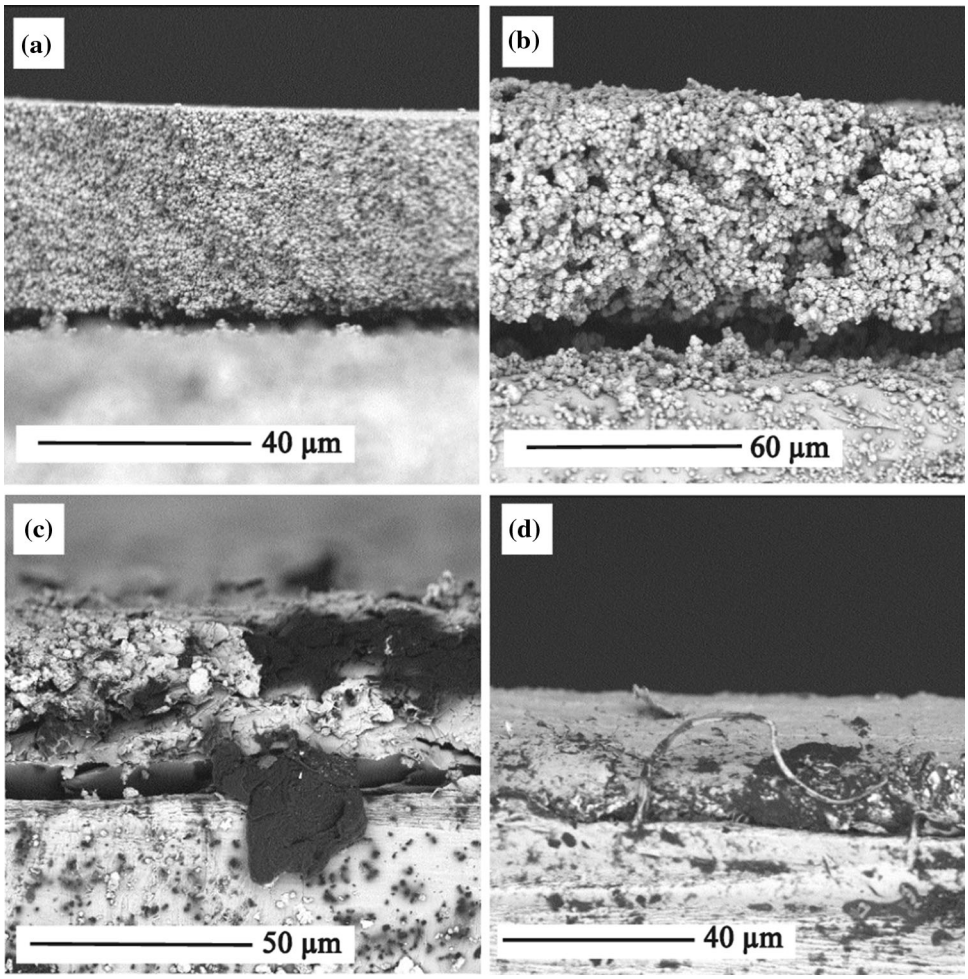

Fig. 4. SEM cross-sectional images of printed films: (a) Ni-1, (b) Ni-2, (c) C, and (d) Ag.

The carbon and nickel films all had similar thickness (C: 47 μm; Ni-1: 40 μm; Ni-2: 53 μm), consistent with their double-pass printing regimen. Silver films, which were printed in a single pass, had approximately half the thickness (18 μm). Of the materials explored, the silver ink produced the highest electrical conductivity film. While this is largely due to silver's higher pure bulk conductivity (10 to 100 times higher than the other bulk materials), we note that the silver film also had the highest density microstructure. This dense microstructure is consistent with the greater fractional conductivity relative to bulk ($\sim$4%) than observed for nickel films ($<$1%). Interestingly, Ni-2 had about five times higher electrical conductivity than Ni-1 despite their similar solids fraction. We again hypothesize that this is largely due to film density. Ni-2's larger particle size (1-μm to 5-μm flakes in Ni-2 versus 1-μm particles in Ni-1) leads to visibly larger aggregates that create greater electrical connectivity across the film.

While the Seebeck coefficient measured from printed films had the same sign as for their bulk counterparts, all values were smaller in magnitude. Among all the printed films, Ni-2 showed the highest magnitude Seebeck coefficient at -5.3 μV/K, whereas silver exhibited the lowest magnitude Seebeck coefficient at 0.6 μV/K. The lower Seebeck coefficient of the films is likely due to the low-density microstructure of the material and the inclusion of polymer binder.

Thermal Behavior

Heat conduction was evaluated using a realistic form factor as described in "Experimental Procedures" section. A representative thermal image of the temperature distribution for a silver film uniformly printed on a square Kapton® substrate is shown in Fig. 5a. Figure 5b aggregates all the data collected in this manner by plotting temperature as a function of distance from the heat source for each film, normalized to the maximum temperature value measured. The experimental error in temperature measurements is below 2% of mean. Figure 5b experimentally demonstrates that the temperature drop across all the film–substrate combinations was nearly identical and equivalent to the control

experiment, an uncoated Kapton® substrate. This result suggests that the electrically conductive coatings did not substantially lower the overall thermal resistance of the polymer substrate. From a practical standpoint, this implies that a large thermal gradient can be maintained, benefiting the performance of a TEG device.

To better understand this thermal behavior, we calculated the thermal resistance for each of the metalized Kapton® substrates; the data shown in Table II are purely estimated thermal resistances based on the electrical conductivity measured from the samples. Even though the thermal resistivity is expected to follow the same trend as the electrical conductivity for each film, it is useful for estimating the total thermal resistance of each film–Kapton® system to understand the thermal transport in the devices. We assume that the heat flow reaches a steady state and is uniform throughout the film–substrate cross-sectional area. We then use the Wiedemann–Franz law to estimate the thermal conductivity of the electrically conductive films. This equation assumes only an electronic contribution to the thermal conductivity.[29]

$$k = \sigma L T, \tag{2}$$

where k is the thermal conductivity, σ is the electrical conductivity, L is the Lorenz number, and T is temperature. We assumed the Lorenz number to be 2.44×10^{-8} W m^{-1} K^{-1}, which is true for most metals and should be reasonably accurate to within an order of magnitude for our films. The thermal resistance of the conductive films (R_{Film}) was calculated using their thermal conductivities and Eq. 3[30]:

$$R_{\text{Film}} = \frac{l}{kA}. \tag{3}$$

The length (l) and width of each film were both 50 mm, and the thickness is listed in Table I (A = width × thickness). Calculated values for the thermal resistance of each film are reported in the second column of Table II. The Kapton® substrate had thickness of 0.125 mm and thermal conductivity of 0.12 W m^{-1} K^{-1}, corresponding to thermal resistance of 6.67×10^4 K/W.[31] To first order, only the silver film showed significantly lower thermal resistance—more than 10x—than the Kapton® substrate. The carbon and Ni-1 films exhibited higher thermal resistance than the Kapton®, whereas the Ni-2 film showed thermal resistance similar to the Kapton®. Finally, we calculated the thermal resistance for each metalized Kapton® substrate using a simple parallel resistance heat flow model (depicted schematically in Fig. 5b, inset). Mathematically, we inversely sum the thermal resistances of the conductive film (R_{Film}) and Kapton® substrate ($R_{\text{Kapton®}}$) to calculate the total parallel thermal resistance:[32]

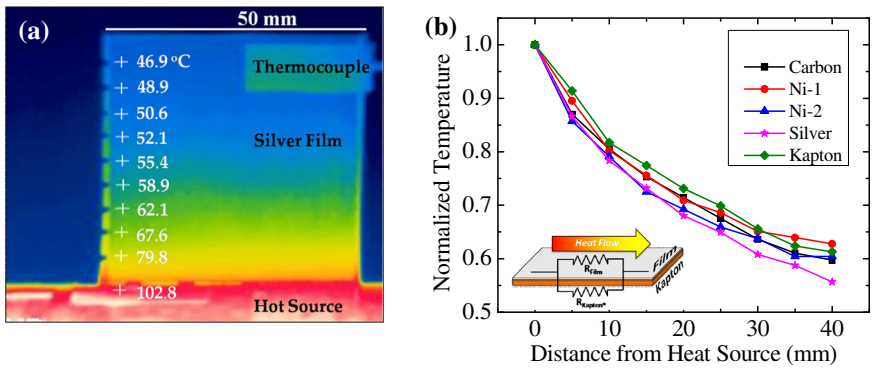

Fig. 5. Thermal profile of printed films: (a) thermal transport in a silver film, (b) thermal transport in printed ink films with distance from heat source.

Table II. Thermal resistance (R) of individual films and parallel resistance of film–Kapton® systems

Film type	Calculated film thermal resistance (K/W)	Film on Kapton®	Calculated thermal resistance for film on kapton® (K/W)
Silver	3.42×10^3	Silver/Kapton®	3.25×10^3
Carbon	2.65×10^6	Carbon/Kapton®	6.50×10^4
Ni-1	1.78×10^5	Ni-1/Kapton®	4.85×10^4
Ni-2	2.73×10^4	Ni-2/Kapton®	1.94×10^4
Kapton®	6.67×10^4	–	–

$$R_{\text{Parallel}} = \frac{R_{\text{Film}} R_{\text{Kapton}}}{R_{\text{Film}} + R_{\text{Kapton}}}. \quad (4)$$

In general, when thermal resistances are added in parallel, the smallest thermal resistance dominates; i.e., heat looks to flow through the path of least resistance. Comparing the values calculated for our system—tabulated in the fourth column of Table II—it is clear that most thermal resistances are of the same order of magnitude as the uncoated Kapton® substrate. Again, only the silver-coated Kapton® substrate deviates significantly (>10× deviation). These results suggest that, as in our experimental data, the heat flow should be similar in most of the metalized Kapton® materials. Interestingly, the lower thermal resistance predicted for the silver-coated Kapton® does not match the observed data. A lower thermal resistance would imply a smaller temperature gradient at steady state, but the data collected in Fig. 5b show a slightly larger (~11%) temperature gradient for the silver-coated Kapton® system. Again, this larger temperature gradient benefits TEG operation, and currently, we suspect that this result is a consequence of more effective convective cooling, though more thorough investigation is needed.

Table III. Measured Seebeck coefficients of junctions compared with values expected based on individual printed films

TEG	Measured $S_A - S_B$ (μV/K)	Expected $S_A - S_B$ (μV/K)
Ag/C	1.5	1.3
Ag/Ni-1	5.1	5.1
Ag/Ni-2	7.5	5.9
C/Ni-1	6.6	6.3
C/Ni-2	9.3	7.1

TEG Device Performance

Finally, the power generation and Seebeck coefficient were evaluated for 31-junction modules. Key performance metrics are reported in Table III. The thermoelectric voltage and power generation for each of the TEG modules were analyzed by increasing the hot-junction temperature from 25°C to 275°C (Fig. 6). The performance of a TEG device over a period of time is shown in Fig. 7. The increase in the electrical resistance for each TEG module with increasing temperature is shown in Fig. 8. This increase in resistance can partially be attributed to the positive temperature coefficient of resistance for the metals. However, the inability to fully recover the film's original electrical conductivity upon cooling suggests that oxidation or other degradation mechanisms are also active. The data are shown in the supporting information (Table S3). As expected from the primary materials assessment, TEGs containing carbon inks exhibited the highest electrical resistances at room temperature. In comparison, the electrical resistance of the Ag/Ni-2 TEG modules was the lowest, suggesting that these inks may be favorable for future development of temperature-stable TEGs. To investigate the robustness of these devices, we tested the Ag/Ni-2 and C/Ni-1 TEGs under continuous operation at 275°C for 3 h. Figure 7 plots the results for the Ag/Ni-2 TEG, demonstrating no loss in performance. We have also demonstrated that, after a year of storage in ambient conditions, these devices retain their performance (see Figs. S3 and S4 in supporting information). We expect the same trend for other devices.

The thermovoltage for TEG junctions was calculated from the measured open-circuit voltages (Fig. 6) and compared with expectations based on the Seebeck coefficients measured for the single materials (Table I). Thus, the calculated values in column 3 of Table III are simply the differences in measured Seebeck coefficients from Table I. C/Ni-2 junctions had the highest thermovoltages, while Ag/C junctions had the lowest. All thermovoltages

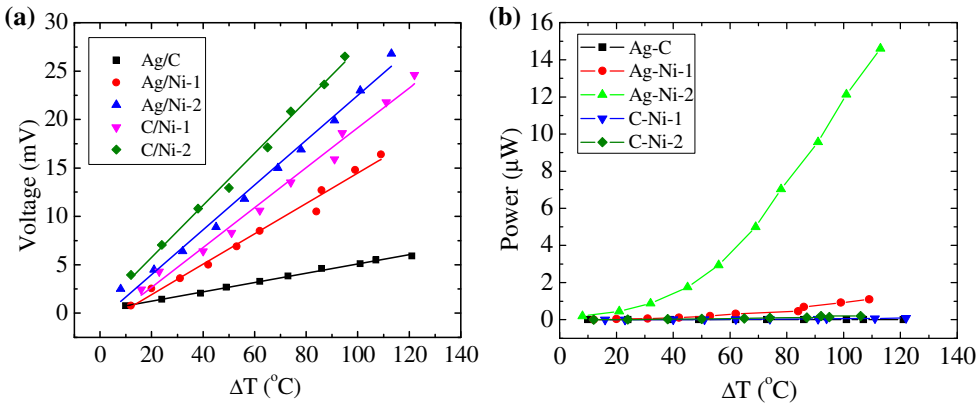

Fig. 6. TEG performance: (a) voltage generated and (b) power produced from TEGs.

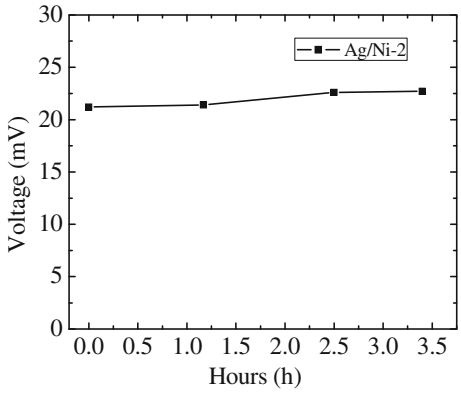

Fig. 7. TEG performance over a period of time at 275°C of constant hot-junction temperature.

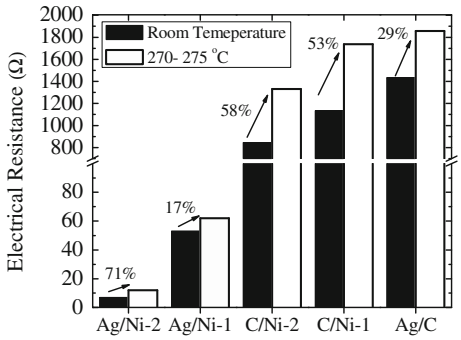

Fig. 8. Electrical resistances of printed TEG devices.

closely matched the expectations based on Seebeck measurements. Variations may be due to differences in measurement temperature as well as the observed degradation of certain materials. However, these results demonstrate that direct measurements of Seebeck coefficient for individual materials are reasonably accurate predictors for thermovoltage values in printed TEG devices.

The thermoelectric power generated from the TEG devices was calculated from measurements of the voltage generated across an equivalent load resistor. The open-circuit voltage and power generation for all devices are plotted as functions of temperature gradient in Fig. 6. TEG modules formed from C/Ni-2 junctions showed the largest open-circuit voltage (35.4 mV at ΔT of 106°C), while the Ag/C TEG showed the lowest open-circuit voltage (5.9 mV at ΔT of 121°C). These results are consistent with the Seebeck coefficient measurements. However, the maximum power was generated from the Ag/Ni-2 TEG (14.6 μW at ΔT of 113°C). This 31-junction device had total length of 22.5 cm, with a corresponding linear power density of 0.65 μW/cm at ΔT of 113°C. Despite its high open-circuit voltage, the high electrical resistance of the C/Ni-2 TEG limited its overall power performance. As expected, evaluation of all transport properties—electrical conductivity, thermal conductivity, and Seebeck effect—is important to predict final TEG performance.

CONCLUSIONS

Important transport properties, including electrical conductivity, thermal conductivity, and Seebeck coefficient, were assessed for conductive thin films prepared from commercially available printed electronic inks. Microstructural features such as void space and particle aggregation size impacted electrical conductivity and Seebeck performance. The relationships between these structural features and key materials properties require further investigation. Thermal conduction for the metalized Kapton® substrates was relatively low ($\Delta T \approx 50$°C over 5 cm) and nearly equivalent to the bare Kapton® material. Using a parallel thermal resistance model, we explain this heat flow behavior by showing that the thermal load of the conductive films is nearly equivalent to the polymer substrate because of the film's small thickness and relatively low electrical conductivity.

Of the screen-printed TEG devices evaluated in this study, the Ag/Ni-2 module showed the highest power output. Linear power production of 0.65 μW/cm was demonstrated for a 31-junction device at ΔT of 113°C. The voltage generated from the silver–nickel TEG was stable during 3 h of continuous operation at 275°C. We have also demonstrated that, after a year of storage in ambient conditions, these devices retain their performance. Despite not having the highest Seebeck difference, the Ag/Ni-2 TEG outperformed all of our other devices due to its low electrical resistance. This result further emphasizes the need for fundamental materials characterization of electronic inks and pastes to further accelerate flexible TEG discovery.

ACKNOWLEDGEMENTS

This work was supported by a grant from North Carolina State University, Raleigh, NC, USA through the 2015 Chancellor Innovation Fund. Authors thank Dr. Philip Bradford (NC State University) for help in sintering the printed samples.

ELECTRONIC SUPPLEMENTARY MATERIAL

The online version of this article (doi: 10.1007/s11664-016-4780-2) contains supplementary material, which is available to authorized users.

REFERENCES

1. I. Johnson, T. William, W. Choate, and A. Amber Davidson, Waste heat recovery: technology and opportunities in US

industry (US Department of Energy, 2008), http://www1.eere.energy.gov/manufacturing/intensiveprocesses/pdfs/waste_heat_recovery.pdf. Accessed 05 December 2015.
2. G.J. Snyder, *Electrochem. Soc. Interface* 17, 54 (2008).
3. S. Jo, M. Kim, M. Kim, and Y. Kim, *Electron. Lett.* 48, 1015 (2012).
4. S.J. Kim, J.H. We, and B.J. Cho, *Energy Environ. Sci.* 7, 1959 (2014).
5. Y. Du, K. Cai, S. Chen, H. Wang, S.Z. Shen, R. Donelson, and T. Lin, *Sci. Rep.* 5, 6411 (2015).
6. D. Madan, Z. Wang, A. Chen, R. Winslow, P.K. Wright, and J.W. Evans, *Appl. Phys. Lett.* 104, 013902 (2014).
7. D. Madan, Z. Wang, A. Chen, P.K. Wright, and J.W. Evans, *ACS Appl. Mater. Interfaces* 5, 11872 (2013).
8. Z. Lu, M. Layani, X. Zhao, L.P. Tan, T. Sun, S. Fan, Q. Yan, S. Magdassi, and H.H. Hng, *Small* 10, 3551 (2014).
9. Z. Cao, E. Koukharenko, R. Torah, J. Tudor, and S. Beeby, *J. Phys.* 01, 2014 (2016).
10. J.H. We, S.J. Kim, G.S. Kim, and B.J. Cho, *J. Alloys Compd.* 552, 107 (2013).
11. S.J. Kim, J.H. We, J.S. Kim, G.S. Kim, and B.J. Cho, *J. Alloys Compd.* 582, 177 (2014).
12. S.K. Yee, S. LeBlanc, K.E. Goodson, and C. Dames, *Energy Environ. Sci.* 6, 2561 (2013).
13. S. LeBlanc, S.K. Yee, M.L. Scullin, C. Dames, and K.E. Goodson, *Renew. Sust. Energy Rev.* 32, 313 (2014).
14. G.G. Yadav, J.A. Susoreny, G. Zhang, H. Yang, and Y. Wu, *Nanoscale* 3, 3555 (2011).
15. T.M. Seeberg, A. Royset, S. Jahren, and F. Strisland, *EMBC: Annual International Conference of the IEEE* (2011), p. 3278.
16. S. Dalola, V. Ferrari, G. Faglia, E. Comini, M. Ferroni, C. Soldano, D. Zappa, and G. Sberveglieri, in *Sensors and Microsystems,* ed. by M. Ferrari (New York: Springer, 2014), p. 3. doi:10.1007/978-3-319-00684-0.
17. D. AgataSkwarek and P. Markowski, *Microelectron. Int.* 31, 176 (2014).
18. K. Suemori, S. Hoshino, and T. Kamata, *Appl. Phys. Lett.* 103, 153902 (2013).
19. Q. Zhang, Y. Sun, W. Xu, and D. Zhu, *Adv. Mater.* 26, 6829 (2014).
20. W. Lee, C.T. Hong, O.H. Kwon, Y. Yoo, Y.H. Kang, J.Y. Lee, S.Y. Cho, K.-S. Jang, and A.C.S. Appl, *Mater. Interfaces* 7, 6550 (2015).
21. J.W. Fergus, *J. Eur. Ceram. Soc.* 32, 525 (2012).
22. F. Jiao, C.-A. Di, Y. Sun, P. Sheng, W. Xu, and D. Zhu, *Phil. Trans. R. Soc. A Math. Phys. Eng. Sci.* 372, 20130008 (2014).
23. Q. Wei, M. Mukaida, K. Kirihara, Y. Naitoh, and T. Ishida, *RSC Adv.* 4, 28802 (2014).
24. DuPont, 5064H silver conductor (DuPont, 2009), www.dupont.com/content/dam/dupont/products…/5064H.pdf. Accessed 10 December 2015.
25. S. Yee, Measurements-electronic properties (www.gatech.edu, 2005), https://sites.google.com/site/yeelabgatech/Measurements/electrical-properties. Accessed 6 December 2015.
26. K. Ankireddy, S. Vunnam, J. Kellar, and W. Cross, *J. Mater. Chem. C* 1, 572 (2013).
27. MatWeb. Material property search (MatWeb, 1996–2016), http://www.matweb.com. Accessed 7 December 2015.
28. C.J.M. Lasance, *Electronics Cooling* (2006), http://www.electronics-cooling.com/2006/11/the-seebeck-coefficient. Accessed 5 December 2015.
29. B.C. Gundrum, D.G. Cahill, and R.S. Averback, *Phys. Rev. B* 72, 245426 (2005).
30. T.L. Bergman, F.P. Incropera, and A.S. Lavine, *Fundamentals of Heat and Mass Transfer*, 7th ed. (Hoboken: Wiley, 2011), p. 22.
31. DuPont, Kapton HN polyimide film (Dupont, 2011), http://www.dupont.com/content/dam/assets/products-and-services/membranes-films/assets/DEC-Kapton-HN-datasheet.pdf. Accessed 10 December 2015.
32. F. Kreith, R. Manglik, and M. Bohn, *Principles of Heat Transfer*, 7th ed. (Stamford: Cengage Learning, 2010), p. 28.